Journal of Natural Gas Science and Engineering 44 (2017) 351–364

Contents lists available at ScienceDirect

Journal of Natural Gas Science and Engineering

journal homepage: www.elsevier.com/locate/jngse

A quick and energy consistent analytical method for predicting hydraulic fracture propagation through heterogeneous layered media and formations with natural fractures: The use of an effective fracture toughness

Oluwafemi Oyedokun*, Jerome Schubert

Department of Petroleum Engineering, Texas A&M University, College Station, TX, USA

ARTICLE INFO

Article history:
Received 30 August 2016
Received in revised form
3 May 2017
Accepted 4 May 2017
Available online 8 May 2017

Keywords:
Effective fracture toughness
Heterogeneous layered media
Hydraulic fracture propagation
Crack closure method
Continuum damage mechanics
Natural fractures

ABSTRACT

An effective fracture toughness, based on equivalent energy release-rate hypothesis is presented for homogenizing heterogeneous layered media. Using crack closure method, the energy released when a mode-1 fracture propagates through an equivalent homogenized layer is equated to the sum of the energies released in the heterogeneous layered media. And from extensive numerical experiments, the predictions of fracture tips' positions through this proposed method are of the same range of accuracy as the known linear blend rule; the weakest link arguments technique performed poorly when compared to the other two methods. Therefore, homogenizing heterogeneous layered media with energy consistent approach will reduce the complexities associated with modeling fracture propagation in multi-layer without losing accuracy. Furthermore, an effective fracture toughness, based on equivalent energy release rate, equivalent strain energy, and modified Kachanov's damage theory is presented in this study. The proposed approach will reduce the computation time required in predicting fracture containment potential in formations with opened or sealed natural fractures. And comparing the proposed phenomenological model with the rigorous solution provided by Mori-Tanaka, it was observed that the margin of error was negligible. The benefit of the proposed phenomenological model over the Mori-Tanaka's effective shear modulus model is the ease of estimating the effective fracture toughness. Thus, these models can be applied to quickly estimate the potential for hydraulic fracture containment or broaching possibilities during oil and gas blowouts and fracturing operations.

Published by Elsevier B.V.

1. Introduction

"Pseudo-3D" (P-3D) models are often used for quick hydraulic fracturing design or prediction of hydraulic fracture containment in the petroleum industry; these models are less computationally expensive compared to the fully 3D and planar 3D models (Morales et al., 1993; Clifton and Abou-Sayed, 1979, 1981; Hirth and Lothe, 1968; Bui, 1977). In the P-3D models, the fluid flow is assumed to be one-dimensional along the length of the fracture, while the pressure profile in each elliptic cross sections is constrained to be linear. And as assumed in the PKN model (Perkins and Kern, 1961; Nordgren, 1972) that the cross sections are independent of each other, so that the plane strain assumption decouples the fluid flow and solid mechanics; similarly, this constraint is applied in the P3D models. The linear pressure profile in the cross sections is based on the assumption that the vertical fracture extension is slow such that the dynamic pressure gradient in the vertical sections is negligible.

Many authors have contributed to the development of the equilibrium height problem (P-3D), starting from the work of Simonson et al. (1978), who developed the model for symmetric 3-layer formation, with constant internal applied pressure. Ahmed (1984), and Newberry et al. (1985) solved an asymmetric 3-layer equilibrium height problem; while Fung et al. (1987) and Economides (2000) extended the asymmetric equilibrium height problem to multi-layer formations with constant and linearly varying pressure profiles in the vertical sections respectively. But as pointed out by Liu and Valko and Liu (2015), the model developed by Economides and Nolte has some intrinsic errors; and sometimes

* Corresponding author.
E-mail addresses: oluwafemi.oyedokun2016@gmail.com (O. Oyedokun), jschubert@tamu.edu (J. Schubert).

http://dx.doi.org/10.1016/j.jngse.2017.05.001
1875-5100/Published by Elsevier B.V.

yield unacceptable results. Other notable contributions to the development of the P-3D models include Palmer and Carroll 1983a,b, Palmer and Craig (1984), Settari and Cleary (1986), Meyer (1986), Advani et al. (1990), and Adachi et al. (2010).

Analytical P-3D model for asymmetric multi-layer formations with linearly varying pressure profile in each cross section is very complicated, and difficult to tract. To reduce the complexity, an effective fracture toughness, based on equivalent energy release rate, developed for the upper and lower layers will condense the multi-layer problem to the classical three-layer problem, which algebra is tractable.

In the same vein, we also proposed in this paper the use of an effective fracture toughness, based on the same hypothesis mentioned earlier, which can approximately describe hydraulic fracture propagation in formations with natural fractures. The interactions between hydraulic and natural fractures have been studied by many authors in the past (Olson and Taleghani, 2009, Zhou et al., 2015; Renshaw and Pollard, 1995; Dahi-Taleghani and Olson, 2011, Gu et al., 2012; Gu and Weng, 2010; Chuprakov et al., 2014, Zhou et al., 2008; Warpinski and Teufel, 1987; Gao and Rice, 1989; Wu, 2014). From the various studies, there are three possibilities that may occur when a hydraulic fracture intersect a natural fracture: (1) the hydraulic fracture may cross the natural fracture without change in propagation direction (2) the hydraulic fracture is arrested by the natural fracture; consequently, the natural fracture, becoming part of the hydraulic fracture network and propagates from its end(s) or (3) from a weak point along its length.

In this study, the complex hydraulic fracture network created by the interactions of the parent hydraulic fracture with ordered and disordered natural fractures will be simplified such that an effective fracture toughness, dependent on area of the discontinuities of a representative volume element and the mechanical properties of the formation matrix can suggest the containment potential of the hydraulic fracture in the host formation.

In past studies, the use of linear blend rule (Atkins, 1979, Atkins and Mai, 1985; Eriksson and Atkins, 1995; Eriksson, 1998) and weakest link arguments (Landes and Shaffer, 1980; Wallin et al., 1984; Slatcher, 1986; Iwadate et al., 1983; Beremin et al., 1983) have been used to homogenize heterogeneous layered media. However, Heerens et al. (1994) showed that the predictions through the weakest link method are inaccurate.

2. Mathematical formulations

2.1. Effective fracture toughness for layered media

Fractures tend to grow in the direction that maximizes the potential energy released. And as a result, most hydraulic fractures propagate in mode-1; although diversion may occur at the boundary of two formations or when intercepted by natural fractures. In this study, the hydraulic fracture is assumed to propagate through boundaries in mode-1 only.

As the hydraulic fracture propagates through each formation, there is an increase in the total energy released; and considering Fig. 1, the total energy released is

$$\Pi_T = \int_{-H_1}^{H_N} \int_0^L G_1 \, dxdz \tag{1}$$

where G_I is the energy release rate, as defined by Griffith (1921). Layers $n+1$ to N can be lumped together as a heterogeneous formation having a varying fracture toughness $K_{c,3}(z)$, while layers 1 to $n-1$ are also lumped together as a heterogeneous formation 1,

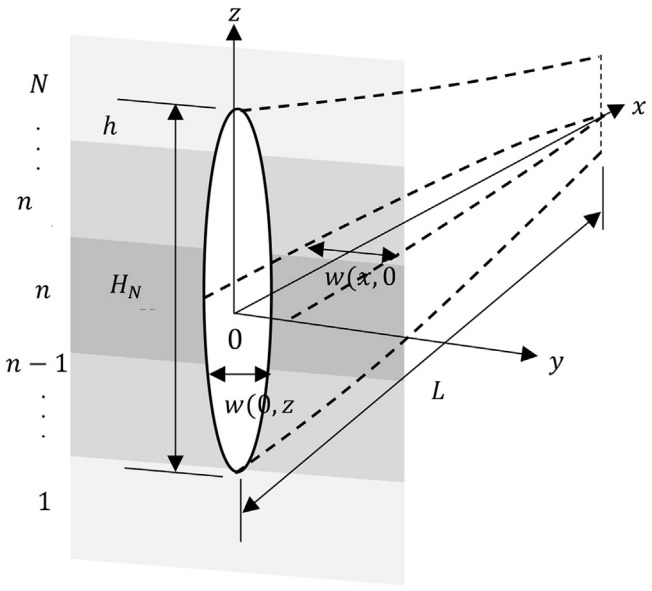

Fig. 1. Asymmetric multilayer hydraulic fracture propagation.

having mode-1 fracture toughness $K_{c,1}(z)$. Therefore, the multi-layer equilibrium-height problem reduces to the classical three-layer problem (Fig. 2).

Assuming the formations have a linearly elastic response, the energy released per unit length of the fracture is

$$\Pi = \int_0^{H_N} G_{1+}(-dz) + \int_0^{H_1} G_{1-} dz \tag{2}$$

Using superposition theorem, the normal stresses at the tips of the vertical fracture plane (in the $y-z$ plane) at arbitrary positions z_0 and z_1 are

$$\sigma_{yy}(z=-z_1) = \sigma_{yy}^{-} = -S_{h\min}(z=z_1) + \frac{K_{I-}}{\sqrt{2\pi(z)}} \tag{3}$$

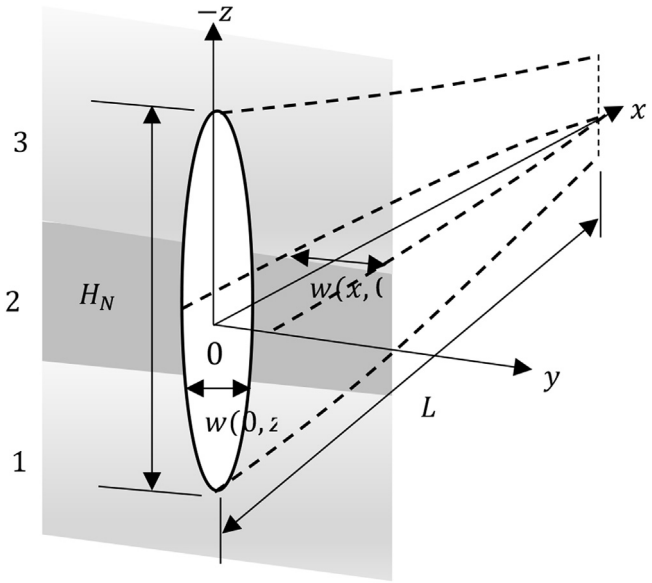

Fig. 2. Asymmetric three-layer equilibrium height problem.

$$\sigma_{yy}(z=z_0)=\sigma_{yy}{}^{+}=-S_{h\min}(z=-z_0)+\frac{K_{I+}}{\sqrt{2\pi(-z)}} \tag{4}$$

with the extension of the upper tip byz_0, new fracture surfaces are created in $0\le z\le z_0$ and the displacement of the upper-right face is

$$u_{yy}{}^{+}=\frac{\kappa+1}{4\mu\pi}K_{I+}\sqrt{2\pi(z_0-z)} \tag{5}$$

Using crack closure method (Irwin, 1958; Broek, 1991), the work done by the normal stress in the fracture extension is equal to the energy required to close the fracture after opening

$$\Pi^{+}=2\int_0^{z_0}\frac{1}{2}\sigma_{yy}{}^{+}u_{yy}{}^{+}dz \tag{6}$$

The factor 2 in Eq.6 accounts for the right and left surfaces of the fracture. And$2u_{yy}{}^{+}(z)=w^{+}(0,z)$. Therefore, the total energy released when the upper fracture tip propagates from the bottom of formation *n+1* to point *h* from the bottom of layer *N* is

$$\begin{aligned}&\sqrt{2\pi}\,\frac{\overline{\kappa}+1}{4\overline{\mu}\pi}\overline{K_{IC}}^{+}\left\{-\frac{2}{3}\left[\sum_{n=1}^{N}S_{h\min,n}(h_{N-1}+h-h_{n-1})^{\frac{3}{2}}-S_{h\min,n}(h_{N-1}+h-h_n)^{\frac{3}{2}}\right]\right\}\\&+\frac{\overline{\kappa}+1}{8\overline{\mu}}\left(\overline{K_{IC}}^{+}\right)^2(h_{N-1}+h)=\left[\sum_{n=1}^{N}-\frac{2\sqrt{2\pi}}{3}S_{h\min,n}\frac{\kappa_n+1}{4\mu_n\pi}K_{IC,n}(h_n-h_{n-1})^{\frac{3}{2}}+\frac{\kappa_n+1}{8\mu_n}K_{IC,n}{}^2(h_n-h_{n-1})\right]\end{aligned} \tag{9}$$

propagates into the abutting layer (lumped), is

$$\overline{\Pi}^{+}=\int_0^{h_{N-1}+h}\sigma_{yy}(z)\frac{\overline{\kappa}+1}{4\overline{\mu}\pi}\overline{K_{Ic}}^{+}(z)\sqrt{2\pi(h-z)}dz \tag{8}$$

Hence, the effective fracture toughness for the lumped upper layer, $\overline{K_{IC}}^{+}$ can be estimated from the hypothesis that $\overline{\Pi}^{+}=\Pi^{+}$. Supposing the in-situ stresses are uniformly distributed throughout each layer, and the upper layers are lumped as a homogeneous formation with fracture toughness, $\overline{K_{IC}}^{+}$, therefore, the effective fracture toughness of the upper layer can be determined from the algebraic expression below. It should be noted that a Heaviside function was used to represent the uniformly distributed in-situ stresses in each layer in Eq. (8) above. And $\overline{\kappa}$ and $\overline{\mu}$ are averaged properties (Poisson ratio function and shear modulus respectively) of the formations; for plane strain approximation, $\overline{\kappa}=3-4\overline{\nu}$ and plane stress $\overline{\kappa}=(3-\overline{\nu})/(1+\overline{\nu})$.

Alternatively, the shear modulus and Poisson ratio can also be represented with Heaviside functions, which will further make Eq. (9) more complicated. Similarly, the effective fracture toughness for the formations below the host formation can be estimated from Eq. 10

$$\begin{aligned}&\sqrt{2\pi}\,\frac{\overline{\kappa}+1}{4\overline{\mu}\pi}\overline{K_{IC}}^{-}\left\{-\frac{2}{3}\left[\sum_{n=1}^{M}S_{h\min,n}(h_{M-1}+h-h_{n-1})^{\frac{3}{2}}-S_{h\min,n}(h_{M-1}+h-h_n)^{\frac{3}{2}}\right]\right\}\\&+\frac{\overline{\kappa}+1}{8\overline{\mu}}\left(\overline{K_{IC}}^{-}\right)^2(h_{M-1}+h)=\left[\sum_{n=1}^{M}-\frac{2\sqrt{2\pi}}{3}S_{h\min,n}\frac{\kappa_n+1}{4\mu_n\pi}K_{IC,n}(h_n-h_{n-1})^{\frac{3}{2}}+\frac{\kappa_n+1}{8\mu_n}K_{IC,n}{}^2(h_n-h_{n-1})\right]\end{aligned} \tag{10}$$

$$\begin{aligned}\Pi^{+}=&\int_0^{h_{n+1}}\sigma_{yy,n+1}\frac{\kappa_{n+1}+1}{4\mu_{n+1}\pi}K_{Ic,n+1}\sqrt{2\pi(h_{n+1}-z)}\,dz\\&+\int_{h_{n+1}}^{h_{n+2}}\sigma_{yy,n+2}\frac{\kappa_{n+2}+1}{4\mu_{n+2}\pi}K_{Ic,n+2}\sqrt{2\pi(h_{n+2}-h_{n+1}-z)}\,dz+\ldots\\&\ldots+\int_{h_{N-1}}^{h_{N-1}+h}\sigma_{yy,N}\frac{\kappa_N+1}{4\mu_N\pi}K_{Ic,N}\sqrt{2\pi(h-z)}dz\end{aligned} \tag{7}$$

Where, the Irwin (1957) criterion, $K_I=K_{IC}$ was implied in Eq. (7). From Fig. 2, the equivalent energy released, as the upper tip

2.2. Effective fracture toughness derivation without tensile stresses

As fracture propagates through each medium, the tensile forces acting on the fracture edges, away from the tips reduces with crack length. Thus, neglecting the tensile force contributions and following the same procedure in Section 2.2 above, the effective fracture toughness for the homogenized upper and lower barriers, based on equivalent energy-release rate hypothesis are derived as

$$\overline{K_{IC}}^{+}=\frac{\sum_{n=1}^{N}\frac{\kappa_n+1}{\mu_n}S_{h\min,n}K_{IC,n}(h_n-h_{n-1})^{\frac{3}{2}}}{\frac{\overline{\kappa}+1}{\overline{\mu}}\sum_{n=1}^{N}S_{h\min,n}\left\{(h_{N-1}+h-h_{n-1})^{\frac{3}{2}}-(h_{N-1}+h-h_n)^{\frac{3}{2}}\right\}} \tag{11}$$

$$\overline{K_{IC}}^{-} = \frac{\sum_{n=1}^{M} \frac{\kappa_n+1}{\mu_n} S_{h\min,n} K_{IC,n} (h_n - h_{n-1})^{\frac{3}{2}}}{\frac{\bar{\kappa}+1}{\bar{\mu}} \sum_{n=1}^{M} S_{h\min,n} \left\{ (h_{M-1} + h - h_{n-1})^{\frac{3}{2}} - (h_{M-1} + h - h_n)^{\frac{3}{2}} \right\}} \tag{12}$$

2.3. Minimum fracture extension pressures

When the pressure driving the hydraulic fracture is assumed to be constant, the fracture extension pressure was derived by Simonson et al. (1978) as

$$P_F = S_{2,h\min}(z) + \frac{K_{IC}}{\sqrt{\pi h_\xi}} \tag{13}$$

where, h_ξ is the half thickness of the host formation. But when the displacements of the upper and lower tips of the fracture are significant, the hydrostatic pressure can significantly affect the extension potential.

The fracture extension pressure may not only be affected by gravity, but the relative positions of the fracture tips can affect the value. Considering the three different cases in Fig. 3. The critical extension pressures for the lower and upper tips in case 1 respectively, as derived in the Appendix are

$$P_{FD} = \left(\frac{\overline{K_{IC}}^{-}}{\sqrt{\pi h_\xi}} + S_{2,h\min} - \frac{1}{2} g h_\xi \rho \right) \tag{14}$$

$$P_{FU} = \left(\frac{\overline{K_{IC}}^{+}}{\sqrt{\pi h_\xi}} + S_{2,h\min} + \frac{1}{2} g h_\xi \rho \right) \tag{15}$$

Noting that $S_{2,h\min}$ is the minimum principal in-situ stress at the host formation. Cases 2 and 3 are not very common; but could be relevant to the extension of existing fractures in formations. In case 2, the critical extension pressures for the upper and lower tips are respectively derived in the **Appendix** as

$$P_{FU} = \frac{2\overline{K_{IC}}^{+}\sqrt{\pi} + \sqrt{h_\xi}\left\{ g h_\xi \pi \rho + 2\left[S_{3,h\min}\sqrt{1-{k_3}^2} + \left(-\sqrt{\frac{1+k_3}{1-k_3}} + k_3\sqrt{\frac{1+k_3}{1-k_3}} + \pi \right) S_{2,h\min} \right] \right\}}{2\sqrt{h_\xi}\left(-\sqrt{\frac{1+k_3}{1-k_3}} + k_3\sqrt{\frac{1+k_3}{1-k_3}} + \sqrt{1-{k_3}^2} + \pi \right)} + \frac{4\sqrt{h_\xi}(S_{3,h\min} - S_{2,h\min})\arcsin\left[\sqrt{\frac{1-k_3}{2}}\right]}{2\sqrt{h_\xi}\left(-\sqrt{\frac{1+k_3}{1-k_3}} + k_3\sqrt{\frac{1+k_3}{1-k_3}} + \sqrt{1-{k_3}^2} + \pi \right)} \tag{16}$$

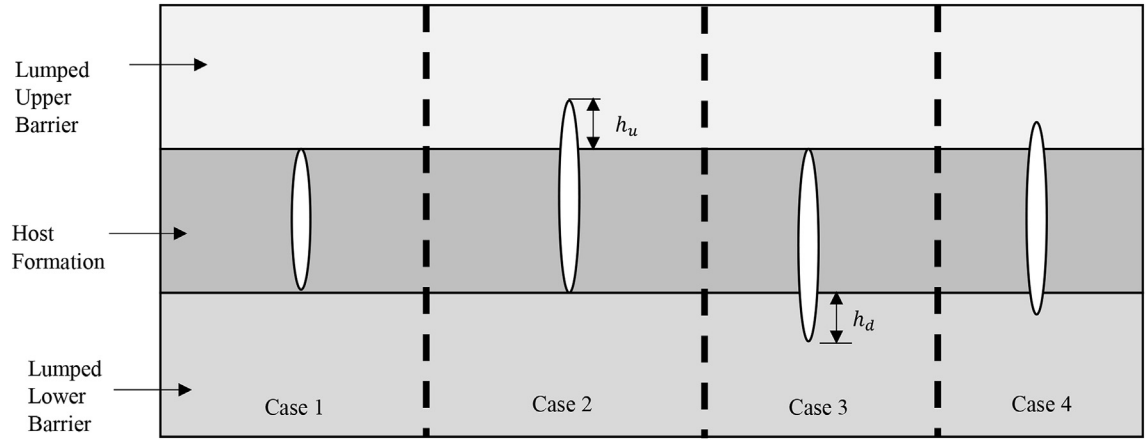

Fig. 3. Possible fracture tips positions in three-layer media.

$$P_{FD} = \frac{\sqrt{k_3+1}\left\{gh_\xi\pi\rho + 2\left[S_{3,h\min}\sqrt{\frac{1-k_3}{1+k_3}}(1+k_3) - \left(\sqrt{\frac{1-k_3}{1+k_3}}k_3 + \sqrt{\frac{1-k_3}{1+k_3}} + \pi\right)S_{2,h\min}\right]\right\}}{2\left\{k_3\left(\sqrt{1-k_3} - \sqrt{\frac{1-k_3}{1+k_3}}\sqrt{1+k_3}\right) + \sqrt{1-k_3} - \sqrt{\frac{1-k_3}{1+k_3}}\sqrt{1+k_3} - \pi\sqrt{1+k_3}\right\}} - \frac{2\overline{K_{IC}}^{-}\sqrt{\pi}\sqrt{\frac{1+k_3}{h_\xi}} - 4\sqrt{k_3+1}(S_{3,h\min} - S_{2,h\min})\arcsin\left[\sqrt{\frac{1-k_3}{2}}\right]}{2\left\{k_3\left(\sqrt{1-k_3} - \sqrt{\frac{1-k_3}{1+k_3}}\sqrt{1+k_3}\right) + \sqrt{1-k_3} - \sqrt{\frac{1-k_3}{1+k_3}}\sqrt{1+k_3} - \pi\sqrt{1+k_3}\right\}} \tag{17}$$

Noting that, $k_3 = \frac{h_\xi}{h_u+h_\xi}$, where h_u is the displacement of the upper tip. For case 3, the critical extension pressures for the upper and lower tips are

$$P_{FU} = \frac{2\overline{K_{IC}}^{+}\sqrt{\pi} + \sqrt{h_\xi}\left\{gh_\xi\pi\rho + 2\left[S_{2,h\min}\sqrt{1-{k_1}^2} - \left(\sqrt{\frac{1-k_1}{1+k_1}} + k_1\sqrt{\frac{1-k_1}{1+k_1}} - \pi\right)S_{1,h\min}\right]\right\}}{2\sqrt{h_\xi}\left(-\sqrt{\frac{1-k_1}{1+k_1}} - k_1\sqrt{\frac{1-k_1}{1+k_1}} + \sqrt{1-{k_1}^2} + \pi\right)} + \frac{4\sqrt{h_\xi}(S_{2,h\min} - S_{1,h\min})\arcsin\left[\sqrt{\frac{1+k_1}{2}}\right]}{2\sqrt{h_\xi}\left(-\sqrt{\frac{1-k_1}{1+k_1}} - k_1\sqrt{\frac{1-k_1}{1+k_1}} + \sqrt{1-{k_1}^2} + \pi\right)} \tag{18}$$

$$P_{FD} = \frac{\sqrt{\frac{\pi}{h_\xi}}\overline{K_{IC}}^{-} - gh_\xi\pi\rho - S_{2,h\min}\sqrt{\frac{1+k_1}{1-k_1}} + k_1S_{2,h\min}\sqrt{\frac{1+k_1}{1-k_1}} + S_{1,h\min}\sqrt{1-{k_1}^2} + \pi S_{1,h\min}}{\left(-\sqrt{\frac{1+k_1}{1-k_1}} + k_1\sqrt{\frac{1+k_1}{1-k_1}} + \sqrt{1-{k_1}^2} + \pi\right)} + \frac{gh_\xi\rho\arcsin\left[\sqrt{\frac{1-k_1}{2}}\right] + \left(gh_\xi\rho + 2S_{2,h\min} - 2S_{1,h\min}\right)\arcsin\left[\sqrt{\frac{1+k_1}{2}}\right]}{2\sqrt{h_\xi}\left(-\sqrt{\frac{1+k_1}{1-k_1}} + k_1\sqrt{\frac{1+k_1}{1-k_1}} + \sqrt{1-{k_1}^2} + \pi\right)} \tag{19}$$

And $k_1 = \frac{h_\xi}{h_d+h_\xi}$.

2.4. Effective fracture toughness for formations with disordered natural fractures

The growth of hydraulic fractures in formations with natural fractures depends on many factors, including the orientation of the micro cracks, the infill materials in the cracks, the tensile strength of the rock, treatment pressure, fluid viscosity, and many other factors as studied by Zhou et al., 2015. To describe the random path of the hydraulic fracture in disordered natural fracture network will be very complicated. But the use of damage theory with the crack closure method (described above) can approximately suggest the containment potential of the hydraulic fracture.

Sometimes the natural fractures may be filled with materials that have higher modulus than the rock matrix; on the other hand the infill materials may have lower Young's modulus than the matrix. The surface density of the cracks and its mechanical strength affect the bearing capacity of the crack-matrix system. If the cracks are filled with higher modulus materials, they help to reinforce the strength of the crack-matrix system; but when the cracks are empty or filled with lower modulus materials, there is a reduction in the bearing capacity of the crack-matrix system. This is the crux of the effective stress introduced by Kachanov (2013); in the classical continuum damage theory, the inclusions are empty; thus, this study will cover both opened and filled discontinuities. For disordered natural fracture network, the impact of the inclinations of the natural fractures to the propagating hydraulic fracture cannot be included in the model development in a deterministic way, except by the use of random theory, which we have decided not to pursue in this paper.

As mentioned in the previous section, the effective fracture

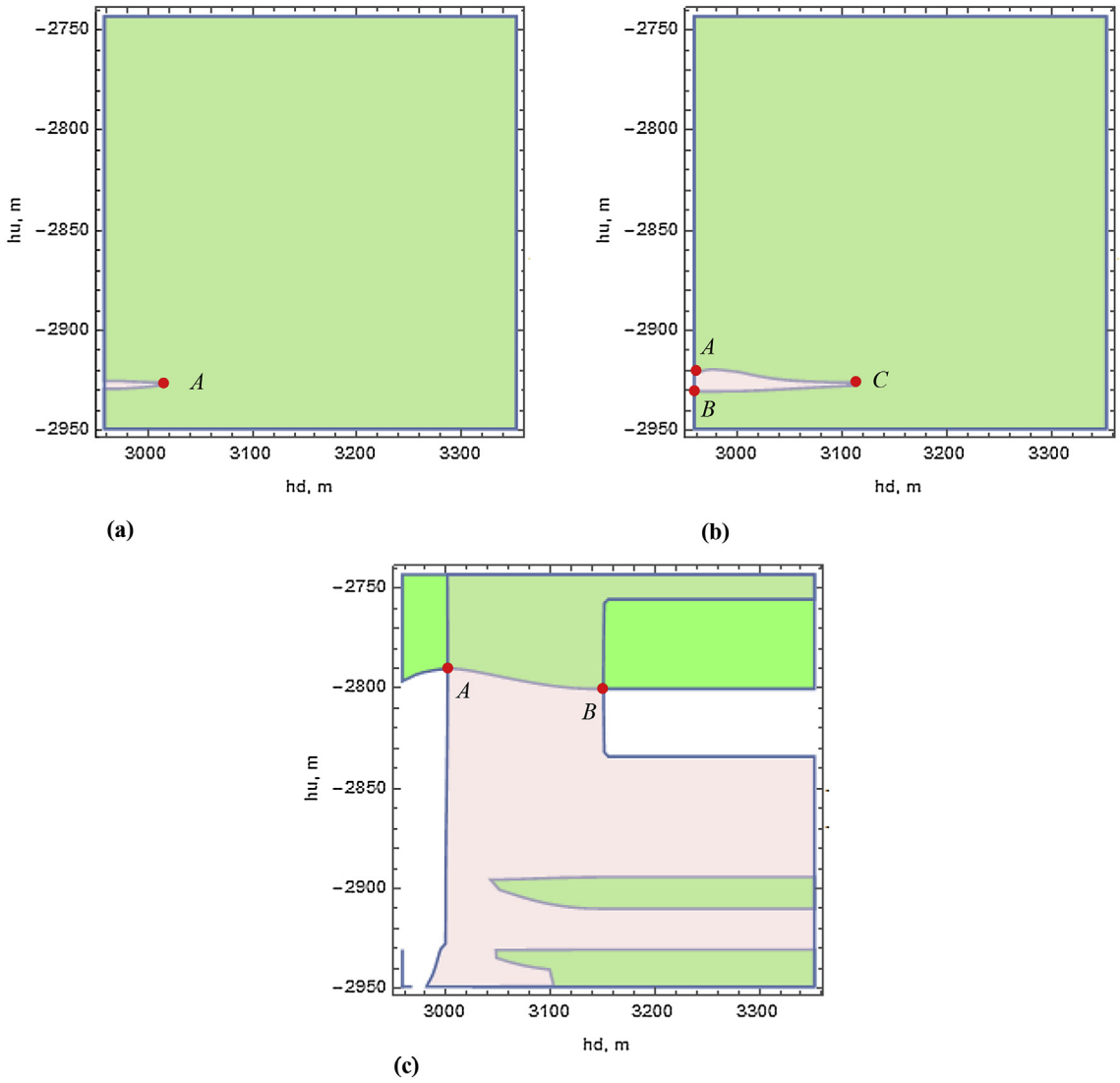

Fig. 4. Region map of the tips positions when the pressure inside the fracture is (a) 53.09 MPa (7700 psi), (b) 53.78 MPa (7800 psi), and (c) 54.47MPa (7900 psi) for 11-EHP.

toughness that describes the containment potential of the hydraulic fracture, propagating in the rock with natural fractures, is based on the use of equivalent energy released rate and equivalent strain energy (by compressional loading) hypotheses. In the equivalent system, the hydraulic fracture network is represented by a mode-1 fracture propagating in a homogeneous medium; and having the same energy released as the fracture propagates to the same height or length. In the equivalent system, the energy released due to mode-2 propagation of the hydraulic fracture is disregarded: when hydraulic fracture is arrested by a natural fracture and consequently the natural fracture propagates from its ends, if the natural fracture is inclined to the direction of maximum in-situ stress in the plane, the propagation will be mixed mode.

The model development are based on the following assumptions:

Assumption 1: The surface discontinuities do not evolve with the applied loadings. This suggest that there is no need to develop an evolution equation for the damage variable, which is the ratio of the effective surface area of the discontinuities in a representative volume element (RVE) and surface area of the RVE.

Assumption 2: The surface discontinuities are isotopically distributed.

Assumption 3: The rock behaves as a linearly elastic material.

Assumption 4: The natural fractures are filled with a material that also has a linearly elastic response.

Table 1
Description of the formation properties and in-situ stress profiles for the 11- eleven problem.

Layer	Top	Thickness	Stress	K_{IC}	E	ν	Lithology
	m.	m.	MPa	MPa$\sqrt{m}$	MPa	–	–
1	2743.200	152.40	52.30	1.10	29,510	0.3	Shale
2	2895.600	30.480	53.99	1.10	29,510	0.3	Shale
3	2926.080	4.572	49.02	1.32	29,510	0.26	Sand
4	2930.652	15.240	54.50	1.10	29,510	0.3	Shale
5	2945.892	3.048	49.34	1.32	29,510	0.26	Sand
6	2948.940	9.144	54.79	1.10	29,510	0.3	Shale
7	2958.084	3.048	49.54	1.32	29,510	0.26	Sand
8	2961.132	4.572	54.97	1.10	29,510	0.3	Shale
9	2965.704	3.048	49.67	1.32	29,510	0.26	Sand
10	2968.752	30.480	55.35	1.10	29,510	0.3	Shale
11	2999.232	152.400	57.05	1.10	29,510	0.3	Shale

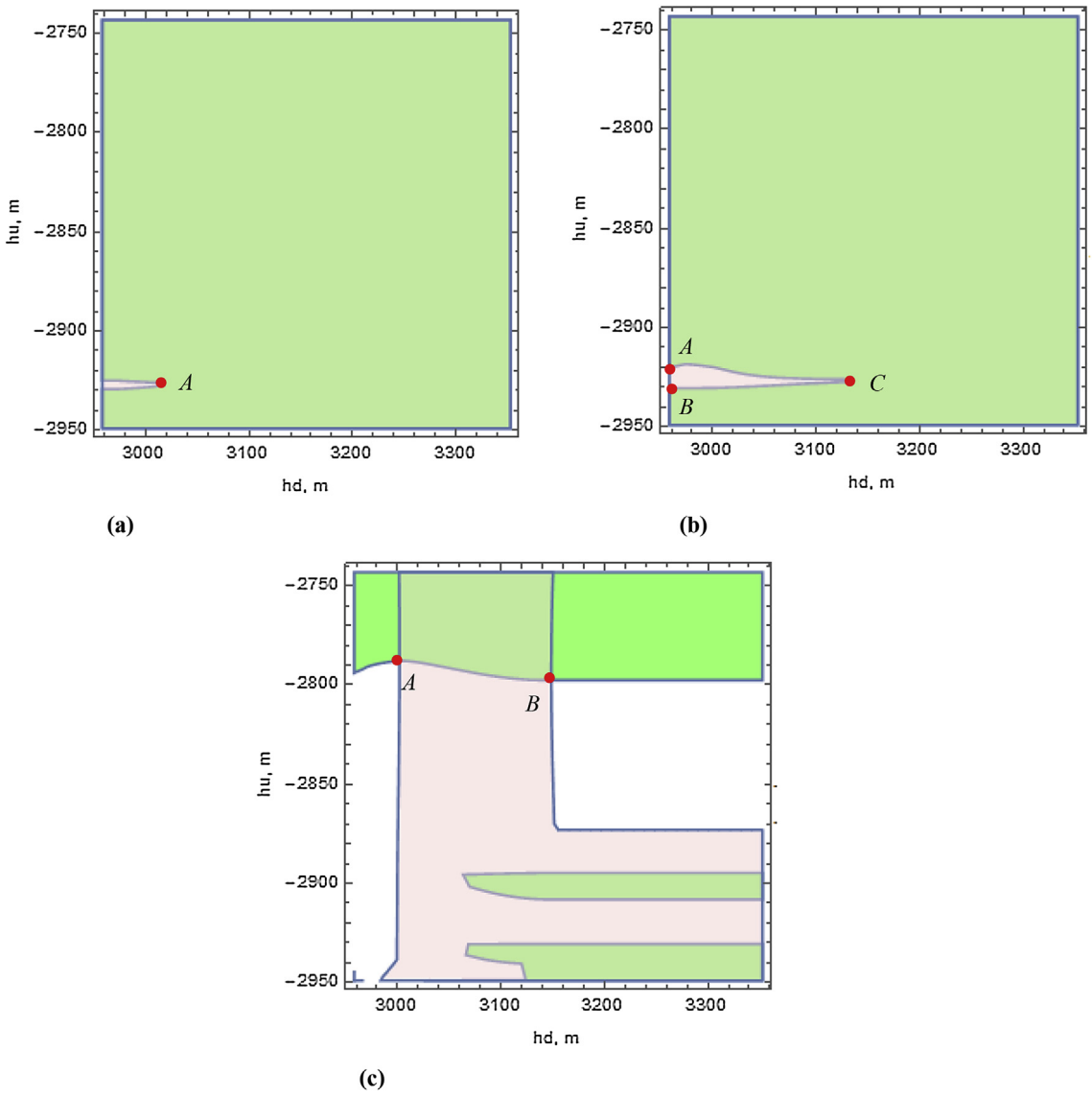

Fig. 5. Region map of the tips positions when the pressure inside the fracture is (a) 53.09 MPa (7700 psi), (b) 53.78 MPa (7800 psi), and (c) 54.47MPa (7900 psi) for 3ER-EHP.

Table 2
Description of the formation properties and in-situ stress profiles for the equivalent three-layer problem.

Layer		Top m.	Thickness m.	Stress MPa	K_{IC} $MPa\sqrt{m}$	E MPa	ν -	Lithology -
3	1	2743.200	152.40	52.30	0.672	29510	0.3	Shaly-Sand
	2	2895.600	30.480	53.99	0.672	29510	0.3	Shaly-Sand
	3	2926.080	4.572	49.02	0.672	29510	0.3	Shaly-Sand
	4	2930.652	15.240	54.50	0.672	29510	0.3	Shaly-Sand
	5	2945.892	3.048	49.34	0.672	29510	0.3	Shaly-Sand
2	6	2948.940	9.144	54.79	1.10	29510	0.3	Shale
1	7	2958.084	3.048	49.54	0.676	29510	0.3	Shaly-Sand
	8	2961.132	4.572	54.97	0.676	29510	0.3	Shaly-Sand
	9	2965.704	3.048	49.67	0.676	29510	0.3	Shaly-Sand
	10	2968.752	30.480	55.35	0.676	29510	0.3	Shaly-Sand
	11	2999.232	152.400	57.05	0.676	29510	0.3	Shaly-Sand

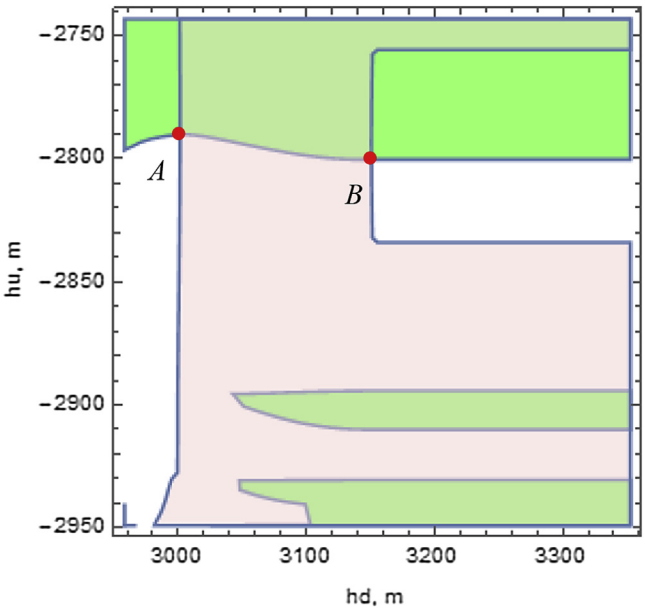

Fig. 6. Region map of the tips positions when the pressure inside the fracture is 54.47MPa (7900 psi) for 3BR-EHP.

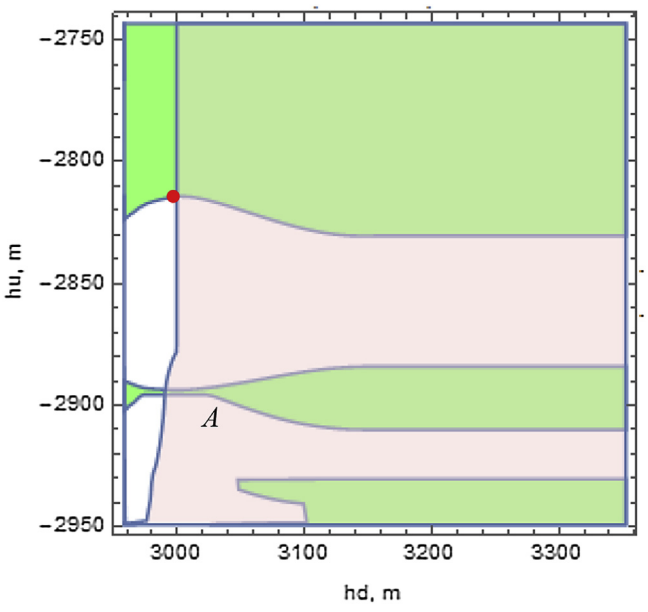

Fig. 8. Region map of the tips positions when the pressure inside the fracture is 54.47MPa (7900 psi) for 11-EHP, Case 2.

The effective stress tensor defined by Kachanov for a material body having empty inclusions is given as

$$\boldsymbol{\sigma}' = \frac{\boldsymbol{\sigma}}{1-\phi} \tag{20}$$

But assuming the filling of the discontinuities reduces its effective area relative to the matrix, then, the effective area of the discontinuities is proposed as

$$S_{\phi,e} = S_{\phi}(1-\lambda)^{\beta} \tag{21}$$

where λ is the ratio of elastic moduli of the infill material and the matrix, and β is a constant parameter. In a case where the infill material has higher elastic modulus than the matrix, then the overall elastic modulus of the inclusion-matrix system will be higher; a reinforcement of the matrix. But the works by Eshelby (1957), Hashin and Shtrikman (1963), Hill (1965), Mori and Tanaka (1973), Willis (1981), Walpole (1981), Weng (1984), and Chen et al. (1992) provide more rigorous studies on the impact of inclusions on the elastic modulus of the host matrix. However, the computation of the effective fracture toughness is demanding (Li and Zhou, 2013).

As stated in **Assumption 1**, the damage variable is defined as

$$D = \frac{S_{\phi,e}}{S} = \phi(1-\lambda)^{\beta} \tag{22}$$

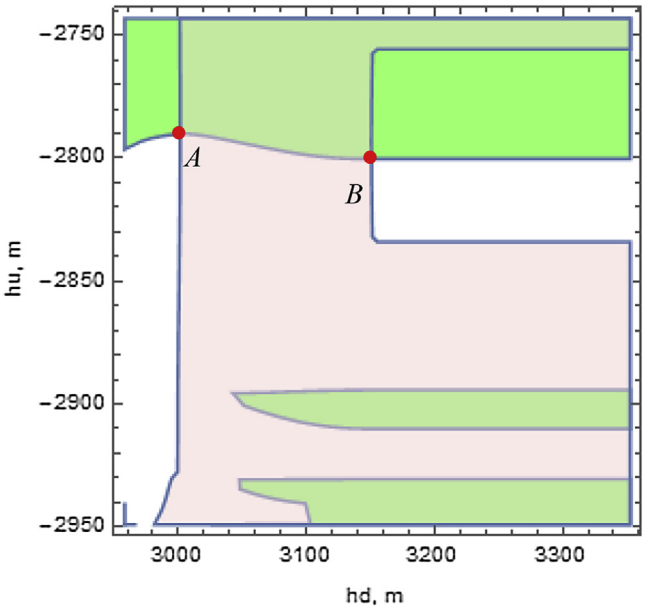

Fig. 7. Region map of the tips positions when the pressure inside the fracture is 54.47MPa (7900 psi) for 3WL-EHP.

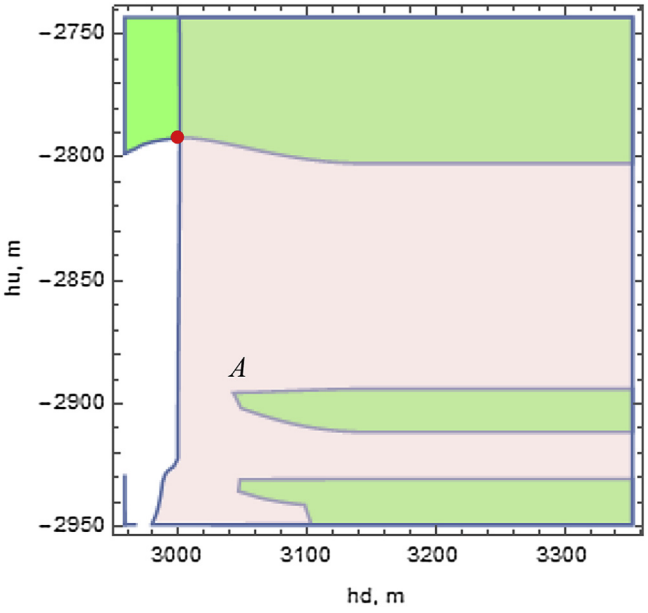

Fig. 9. Region map of the tips positions when the pressure inside the fracture is 54.47MPa (7900 psi) for 3ER-EHP, Case 2.

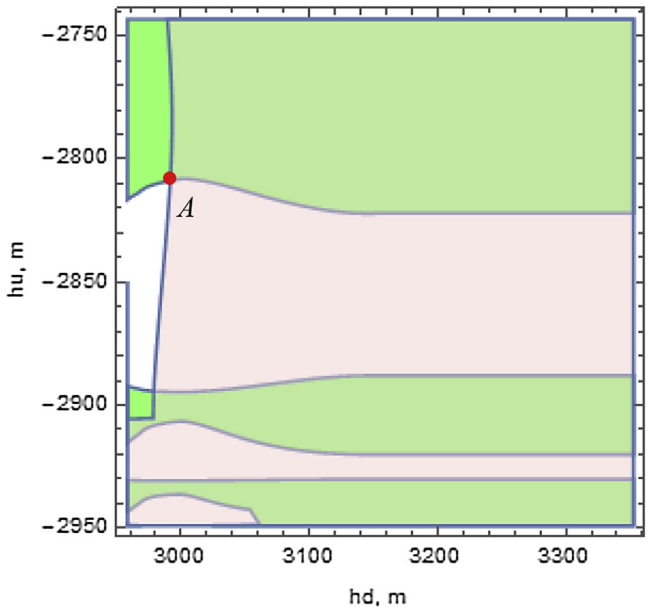

Fig. 10. Region map of the tips positions when the pressure inside the fracture is 54.47MPa (7900 psi) for 3BR-EHP, Case 2.

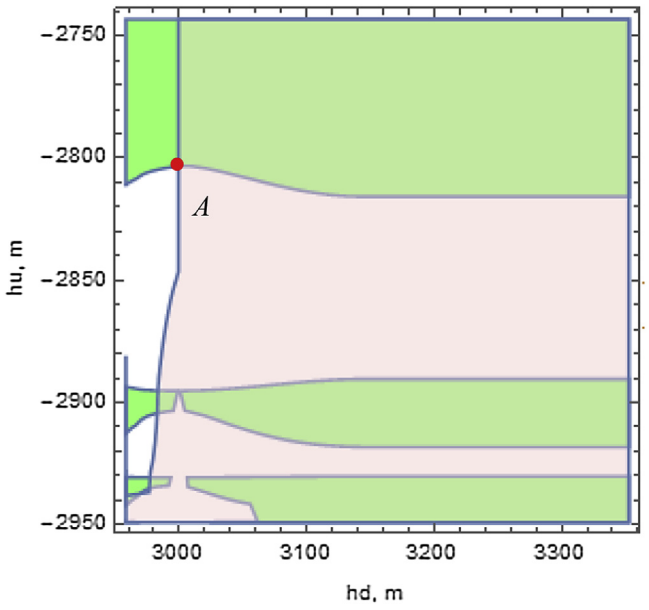

Fig. 12. Region map of the tips positions when the pressure inside the fracture is 54.47MPa (7900 psi) for 3EER-EHP, Case 2.

and using the crack closure method, the energy released in the damaged rock material is equivalent to the energy released in a virgin rock with the normal stress acting on the face of the fracture being the effective stress, i.e.

$$\Pi = 2\int_0^{z_0} \frac{1}{2}\sigma_{yy}u_{yy}dz = 2\int_0^{z_0} \frac{1}{2}\sigma'_{yy}u'_{yy}dz \tag{23}$$

Where,

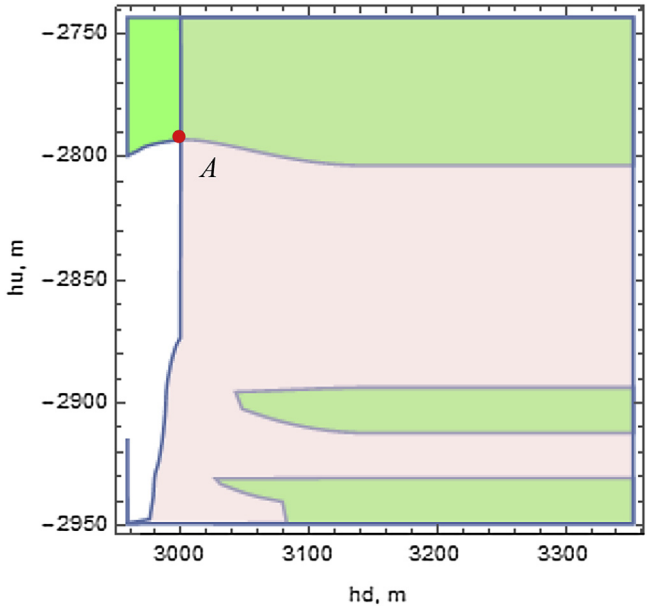

Fig. 11. Region map of the tips positions when the pressure inside the fracture is 54.47MPa (7900 psi) for 3WL-EHP, Case 2.

$$u'_{yy} = \frac{\kappa' + 1}{4\mu'\pi}K'_{IC}\sqrt{2\pi(z_0 - z)} \tag{24}$$

and,

$$\sigma'_{yy} = -S'_{h\min} + \frac{K'_{IC}}{\sqrt{2\pi z}} \tag{25}$$

$$u_{yy} = \frac{\kappa + 1}{4\mu\pi}K_{IC}\sqrt{2\pi(z_0 - z)} \tag{26}$$

$$\sigma_{yy} = -S_{h\min} + \frac{K_{IC}}{\sqrt{2\pi z}} \tag{27}$$

by substituting equations 22–25 into (21), the effective fracture toughness can be determined from the algebraic expression

$$\frac{\kappa' + 1}{\mu'}K'_{IC}\left(-\frac{2}{3}S'_{h\min}z_0^{3/2} + \frac{K'_{IC}}{\sqrt{2\pi}}\frac{\pi}{2}z_0\right) = \frac{\kappa + 1}{\mu}K_{IC}\left(-\frac{2}{3}S_{h\min}z_0^{3/2} + \frac{K_{IC}}{\sqrt{2\pi}}\frac{\pi}{2}z_0\right) \tag{28}$$

Table 3
Description of the formation properties and in-situ stress profiles for the 11-EHP, Case 2.

Layer	Top	Thickness	Stress	K_{IC}	E	ν	Lithology
	m.	m.	MPa	MPa$\sqrt{m}$	MPa	–	–
1	2743.200	152.40	52.30	5.10	29,510	0.3	Shale
2	2895.600	30.480	53.99	1.10	29,510	0.3	Sand
3	2926.080	4.572	49.02	3.32	29,510	0.26	Shale
4	2930.652	15.240	54.50	1.10	29,510	0.3	Shale
5	2945.892	3.048	49.34	5.32	29,510	0.26	Shale
6	2948.940	9.144	54.79	1.10	29,510	0.3	Shale
7	2958.084	3.048	49.54	6.32	29,510	0.26	Sand
8	2961.132	4.572	54.97	2.10	29,510	0.3	Shale
9	2965.704	3.048	49.67	1.32	29,510	0.26	Sand
10	2968.752	30.480	55.35	3.10	29,510	0.3	Shale
11	2999.232	152.400	57.05	6.10	29,510	0.3	Shale

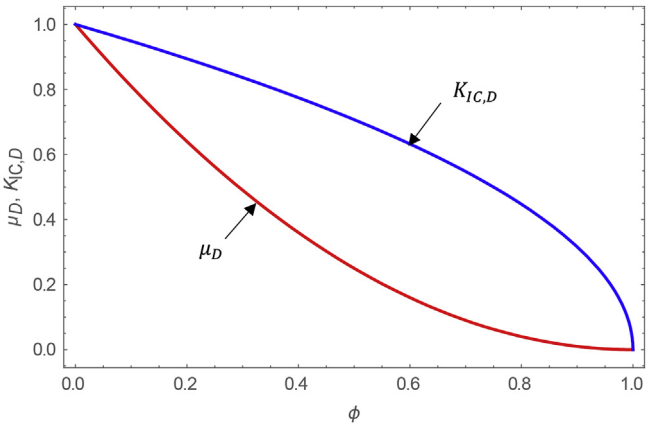

Fig. 13. Variations of the normalized shear modulusμ_D, and normalized fracture toughness with damage in any material displaying a linear elastic response. $\lambda = 0$ in this case.

Since damage prior to loading is under consideration and not damage induced by the loading; thus, considering a compression loading of the RVE. The elastic strain energy (compressional loading) and the effective elastic energy are equivalent, i.e.

$$\frac{1}{2}\int_{B} \boldsymbol{\sigma}\boldsymbol{\varepsilon} dv = \frac{1}{2}\int_{B'} \boldsymbol{\sigma}'\boldsymbol{\varepsilon}' dv' \tag{29}$$

Hence, the relationship between the damaged and virgin shear moduli is

$$\mu = \mu'\left[1 - \phi(1-\lambda)^{\beta}\right]^2 \tag{30}$$

The constant parameterβ, can be determined by curve-fitting the effective shear modulus in Eq. (30) with Mori-Tanaka's model or from experiment.

When the contributions of the tensile stresses along the fracture edges are disregarded, the damaged fracture toughness of the formation becomes

$$K_{IC} = K'_{IC}\sqrt{1 - \phi(1-\lambda)^{\beta}} \tag{31}$$

2.5. Effective fracture toughness for formations with ordered natural fractures

When the natural fractures are oriented in the same direction, the path of the main hydraulic fracture stem can be easily traced compared to the disordered pattern. In this case the energy released as the fracture propagates in both modes 1 and 2 is

$$\Pi = 2\int_{c} \frac{1}{2}\sigma_{yy}u_{yy}\, ds + \int_{c_2} 2N\frac{1}{2}\sigma_{xy}u_{xx} ds_2 = 2\int_{0}^{z_0} \frac{1}{2}\sigma'_{yy}u'_{yy} dz \tag{32}$$

Where, c is the path of the main hydraulic fracture, and c_2 is the distance the fracture propagates in mixed mode. N is the number of repeated pattern of the natural fractures; in other words, the number of rows. Eq. (32) is derived based on the assumption that the natural fracture will propagate from one of its ends, when it arrests the hydraulic fracture.

$$u_{xx} = \frac{\kappa + 1}{4\mu\pi} K_{IIC}\sqrt{2\pi(z_0 - z)} \tag{33}$$

$$\sigma_{xy} = \frac{K_{IIC}}{\sqrt{2\pi z}} \tag{34}$$

Depending on the projected path, the steps in Section 2.3 can be followed in estimating the effective fracture toughness from equation (32).

3. Numerical examples

A hydraulic fracture stands in layer 6, with its tips at the top and bottom of the formation, which is 9 m (30 ft) thick. Using the full multi-layer equilibrium height model, the tips displacements at different internal pressures are shown in Fig. 4a b, and c. Table 1 shows the description of the layers. While the use of the energy-released-based effective fracture toughness for the same range of pressures are shown in Fig. 5a, b, and c.

The equivalent three-layer system, based on equivalent energy release rate hypothesis, (3ER-EHP) to the eleven-layer problem (11-EHP) is shown in Table 2 below. Comparing the region maps in Fig. 4a,b and c and Fig. 5a and b, and 5c, it is evident that the two solutions are equivalent. Points A, B, and C in Fig. 4a, b, 5a, and 5b

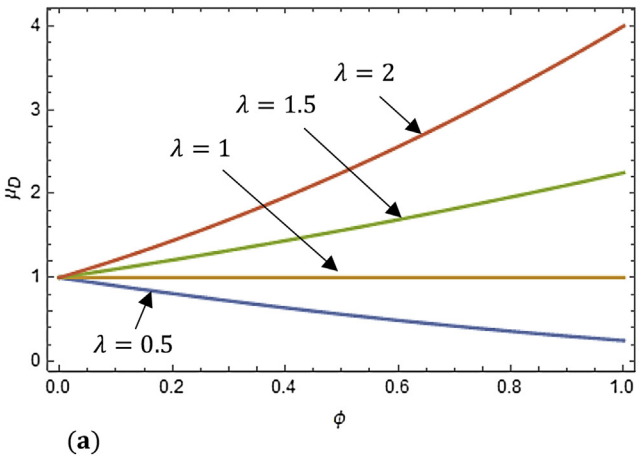

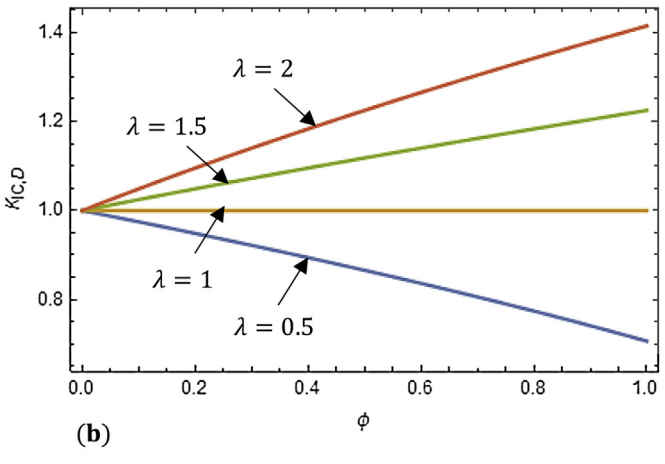

Fig. 14. (a) Variation of the normalized shear modulusμ_D, considering different infill materials (b) Variation of normalized fracture toughness, $K_{IC,D}$, with damage considering different infill materials.

Table 4
Elastic properties of the matrix and inclusions.

Case	Matrix Young's Mod.	Infill Young's Mod.	Matrix Poisson Ratio	Infill Poisson Ratio
	GPa.	GPa	–	–
1	29.5	0	0.3	0
2	29.5	5.0	0.3	0.33
3	20.0	25.0	0.26	0.25

are not the practical solutions to the nonlinear equation; at these pressure values, the initial upper and lower tips are stable. In Figs. 4c and 5c Point B is the pair solution to the practical solution A. From the map, the upper tip is located at depth 2790 m, while the lower tip is located at depth 3005 m.

Using the linear blend rule and weakest link arguments, the effective fracture toughness for the upper and lower barriers are 1.11 MPa and 1.1 MPa respectively. The locations of the tips in these equivalent systems are similar to the 3ER-EHP (Fig. 6 and 7); for shorthand writing, the equivalent three layer problem based on blend rule is 3BR-EHP, and that based on weakest link arguments is 3WL-EHP. In this case, both 3ER-EHP and 3WL-EHP yielded similar results, while 3BR-EHP and 3ERR-EHP gave more accurate positions of the tips relative to the other homogenization methods (Figs. 8–12).

From these examples, it is evident that the use of energy-release rate hypothesis for homogenizing multilayer problems may not be accurate (to a small degree), except when the contributions of the tensile stresses are neglected.

Table 3 shows the description of eleven layers with significant modulus contrasts. And the effective fracture toughness for the upper and lower barriers using the equivalent energy release rate hypothesis are 1.44MPa and 1.59 MPa respectively. While the effective fracture toughness for the upper and lower homogenized barriers when using the linear blend rule are 4.17 MPa and 5.46 MPa respectively; and using the weakest point arguments, the effective fracture toughness are 1.6MPa and 3.28MPa respectively. In the same vein, the effective fracture toughness using the reduced equivalent energy release rate hypothesis (3ERR-EHP) are 3.38MPa and 4.15 MPa respectively.

Alternatively, the use of equivalent strain energy hypothesis, which is mathematically tedious, may be used in lieu of the energy released rate; this comparison will not be pursued in this paper.

The tensile stress is greatest at the tips of the fracture, and reduces along the length of the fracture. Along the edges of the fracture, away from the tips, the Irwin criterion, $K_I = K_{IC}$, does not apply; but $K_I < K_{IC}$. Thus, neglecting the tensile stress contribution in the crack closure energy function will yield more accurate results; and this is evident in the two example cases.

Fig. 13 shows that the impact of damage on the elastic properties of the formation matrix do not follow the same path. The Young's and shear moduli are more severely damaged than the fracture toughness. And based on isotropic damage assumption, the Poisson

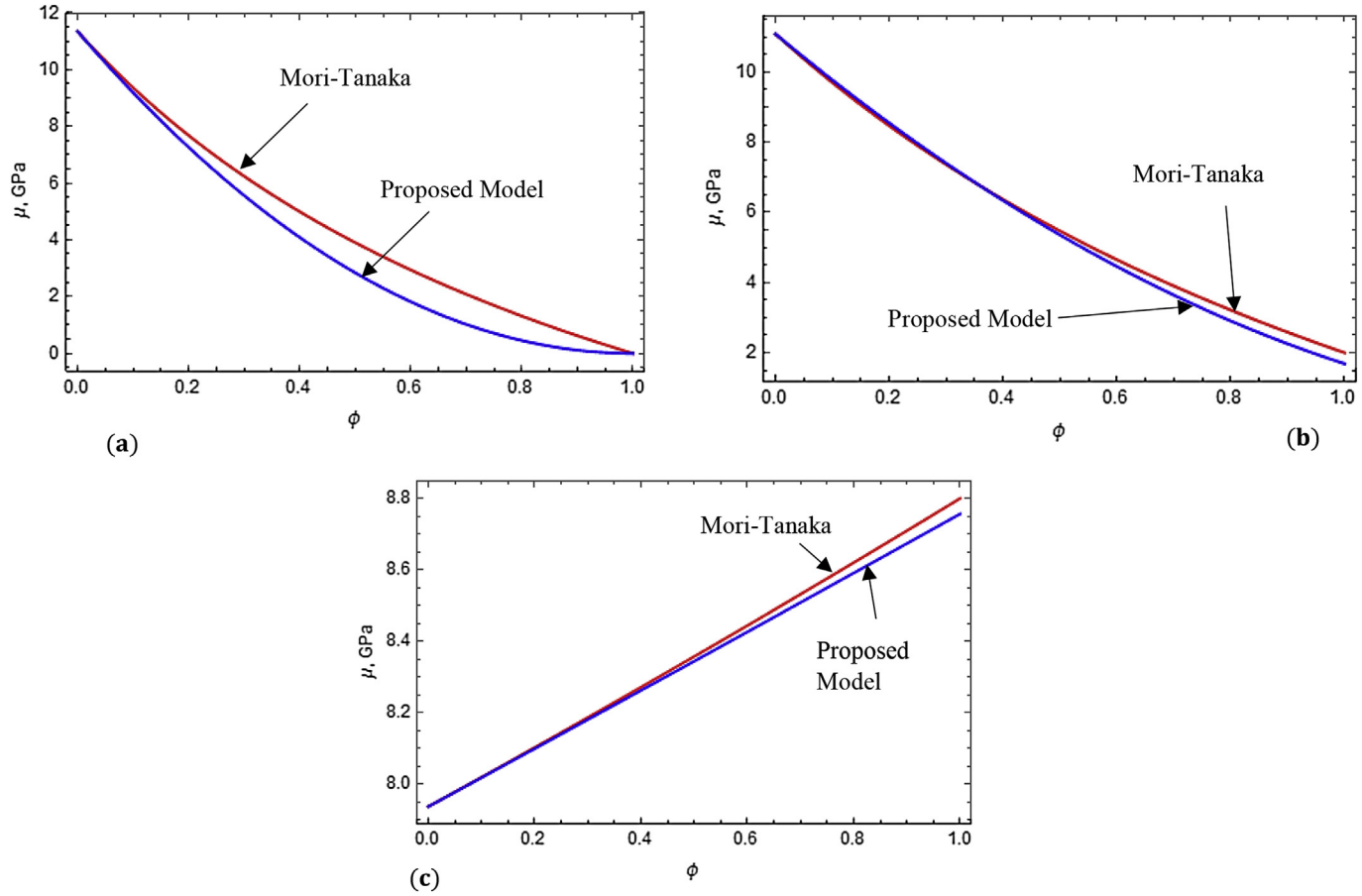

Fig. 15. Comparing the performance of the proposed model for effective shear modulus of a material body having (a) empty or open natural fractures, Case 1, (b) micro-fractures filled with lower modulus material, Case 2, and (c) micro-fractures filled with higher modulus material, Case 3.

ratio will not be affected by the presence of the discontinuities (damage), based on the continuum damage theory; the impact of damage on other elastic properties are beyond the scope of this article. And Fig. 14a and b, show the variations of the effective shear modulus and fracture toughness when the discontinuities (inclusions, or natural fractures) are filled with material having lower or higher Young's modulus.

To compare the predictions of the proposed effective shear modulus for the damaged/reinforced material with Mori-Tanaka's model, Table 4 shows the three cases:

As observed in Fig. 15a, the prediction from the proposed phenomenological model mimics the rigorous Mori-Tanaka model. In the second and third cases, the values of β are 2.5 and 1.2 respectively.

4. Summary

Using equivalent energy release-rate hypothesis, an effective fracture toughness was derived to homogenize heterogeneous layered media. Homogenizing heterogeneous layered media into a single layer can reduce multi-layer equilibrium-height problem to the classical three-layer equilibrium-height problem. And the reduction of the multi-layer problem to the classical three-layer problem reduces the model complexity. The predictions from the proposed model have the same range of accuracy as the well-known linear blend rule; while the predictions from the weakest link arguments method were also observed to be inaccurate.

Furthermore, an effective fracture toughness formulation for predicting the growth of hydraulic fracture in a formation with micro-cracks or any other form of ordered or disordered inclusions was developed. The formulation is based on the use of damage theory, equivalent energy-release rate, and equivalent strain-energy hypotheses. The presence of infill materials in the micro-cracks (closed natural fractures) will affect the overall elastic properties of the damaged/reinforced rock-fracture system. And using a phenomenological approach, which is based on the use of an effective area, the proposed model performs very well as the rigorous Mori-Tanaka model, when the fractures are open. Then using the Mori-Tanaka model for the effective shear modulus, as reference, the constant parameter in the proposed model can be determined; subsequently, estimating the effective fracture toughness for the rock-closed fracture system. The benefit of the proposed model over the Mori-Tanaka is its simplicity in computing the effective fracture toughness.

Acknowledgement

This research is primarily supported by the Blowout Risk Assessment Joint Industry Projects.

Nomenclature

D	damage variable	P_{FD}	minimum fracture extension pressure for lower tip
G_{I+}	energy release rate in upper barriers	$S_{h,min}$	minimum horizontal in-situ stress
G_{I-}	energy release rate in lower barriers	$u_{yy}{}^{+}$	fracture half width in the upper barriers
h_u	displacement of the upper tip	$u_{yy}{}^{-}$	fracture half width in the lower barriers
h_d	displacement of the lower tip	μ_n	formation, n, shear modulus
K_{I+}	stress intensity factor at upper tip	$\overline{\mu}_u$	Averaged shear modulus for upper barriers
K_{I-}	stress intensity factor at lower tip	$\overline{\mu}_d$	Averaged shear modulus for lower barriers
$\overline{K}_{IC}{}^{+}$	effective fracture toughness for upper homogenized upper barriers	λ	ratio of inclusion and undamaged matrix elastic moduli
$\overline{K}_{IC}{}^{-}$	effective fracture toughness for homogenized lower barriers	ϕ	Ratio of the surface area of discontinuity to surface area of representative volume element
P_{FU}	minimum fracture extension pressure for upper tip		

Appendix. Derivation of minimum fracture propagation for three-layer problem

Sneddon and Elliott (1946) derived the stress intensity factor at the tip of a fracture subjected to a constant internal pressure. Modifying the equation by including the effect of gravity, the stress intensity factor at the bottom tip, when the fracture is contained in formation n only:

$$K_{I,D} = \frac{1}{\sqrt{\pi l}} \int_{-l}^{z} p(z,t) - \sigma_n \sqrt{\frac{l+z}{l-z}} dz \tag{A.1}$$

$$\text{Let } z^* = \frac{z}{l} \tag{A.2}$$

$$\text{And at } \left.\begin{matrix} z = z, z^* = z^* \\ z = -l, z^* = -1 \end{matrix}\right\} \tag{A.3}$$

$$\frac{dz^*}{dz} = \frac{1}{l} \tag{A.4}$$

Substituting (A.3) and (A.4) into (A.1),

$$K_{I,D} = \sqrt{\frac{l}{\pi}} \int_{-1}^{z^*} (p_Q(t) + \rho g l z^* - \sigma_n) \sqrt{\frac{1+z^*}{1-z^*}} dz^* \tag{A.5}$$

Solving (A.5) and substituting (A.2) back yields

$$\begin{aligned} K_{I,D} = \frac{1}{2\sqrt{\pi}\sqrt{l(l-z)}} \Big\{ & -(l-z)\sqrt{l+z}(g(2l+z)\rho - 2\sigma_n) \\ & + 2l\sqrt{l-z}\,(gl\rho - 2\sigma_n)\sin^{-1}\left(\frac{\sqrt{\frac{l+z}{l}}}{\sqrt{2}}\right) \\ & + p_Q\left(2(-l+z)\sqrt{l+z} + 4l\sqrt{l-z}\sin^{-1}\left(\frac{\sqrt{\frac{l+z}{l}}}{\sqrt{2}}\right)\right)\Big\} \end{aligned} \tag{A.6}$$

$$\lim_{z\to l}\{K_{I,D}\} = \frac{\sqrt{l\pi}}{2}(gl\rho + 2p_Q - 2\sigma_n) \tag{A.7}$$

Therefore, the critical pressure at the mid position Q to cause the lower tip to move is

$$p_Q = P_{FD} = \left(\frac{K_{IC,D}}{\sqrt{\pi l}} + \sigma_n - \frac{1}{2}gl\rho\right) \tag{A.8}$$

At the upper tip, the stress intensity factor is

$$K_{I,U} = \frac{1}{\sqrt{\pi l}} \int_{-l}^{z} p(z,t) - \sigma_n \sqrt{\frac{l-z}{l+z}} dz \tag{A.9}$$

$$\text{Let } z^* = -\frac{z}{l} \tag{A.10}$$

$$\text{And at } \begin{matrix} z = z, z^* = -z^* \\ z = -l, z^* = 1 \end{matrix} \Bigg\} \tag{A.11}$$

$$\frac{dz^*}{dz} = -\frac{1}{l} \tag{A.12}$$

Substituting (A.11) and (A.12) into (A.9),

$$K_{I,U} = \sqrt{\frac{l}{\pi}} \int_{-z^*}^{1} (p_Q(t) - \rho g l z^* - \sigma_n)\sqrt{\frac{1+z^*}{1-z^*}} dz^* \tag{A.13}$$

Solving (A.13) and substituting (A.2) back yields

$$\begin{aligned} K_{I,U} = \frac{1}{2\sqrt{\pi}\sqrt{l(l-z)}} \Bigg\{ & -(l-z)\sqrt{(l+z)}(g(2l+z)\rho + 2\sigma_n) \\ & - 2l\sqrt{(l-z)}\,(gl\rho + 2\sigma_n)\cos^{-1}\left(\frac{\sqrt{\frac{l+z}{l}}}{\sqrt{2}}\right) \\ & + 2p_Q\left((l-z)\sqrt{(l+z)} + 2l\sqrt{(l-z)}\cos^{-1}\left(\frac{\sqrt{\frac{l+z}{l}}}{\sqrt{2}}\right)\right)\Bigg\} \end{aligned} \tag{A.14}$$

$$\lim_{z\to l}\{K_{I,U}\} = \frac{\sqrt{l\pi}}{2}(-gl\rho + 2p_Q - 2\sigma_n) \tag{A.15}$$

Therefore, the critical pressure at midpoint Q to cause the upper tip to move is

$$p_Q = P_{FU} = \left(\frac{K_{IC,U}}{\sqrt{\pi l}} + \sigma_n + \frac{1}{2}gl\rho\right) \tag{A.16}$$

Noting that $l = h_\xi$. Hence, extending the derivation to three layer: the stress intensity factor at the upper tip is

$$\begin{aligned} K_{I,U} = \frac{1}{\sqrt{\pi l}} \Bigg\{ & \int_{-k_3}^{1} (p_Q(t) - \rho g l z^* - \sigma_3)\sqrt{\frac{1+z^*}{1-z^*}} dz^* \\ & + \int_{-k_1}^{-k_3} (p_Q(t) - \rho g l z^* - \sigma_2)\sqrt{\frac{1+z^*}{1-z^*}} dz^* \\ & + \int_{-z^*}^{-k_1} (p_Q(t) - \rho g l z^* - \sigma_1)\sqrt{\frac{1+z^*}{1-z^*}} dz^* \Bigg\}_{z\to l} \end{aligned} \tag{A.17}$$

Therefore, the minimum fracture extension pressure for the upper tip at any location z is p_Q in (A.17); since the algebraic expression is complicated, it will not be displayed in this paper. In the same vein, when k_1 approaches unity, the fracture extension pressure for the upper tip corresponds to case 2 in Fig. 3. And when k_3 approaches unity, the fracture extension pressure for the upper tip corresponds to case 3 in Fig. 3.

Similarly, the stress intensity factor at the lower tip is

$$\begin{aligned} K_{I,D} = \frac{1}{\sqrt{\pi l}} \Bigg\{ & \int_{-1}^{k_3} (p_Q(t) + \rho g l z^* - \sigma_3)\sqrt{\frac{1+z^*}{1-z^*}} dz^* \\ & + \int_{k_3}^{k_1} (p_Q(t) + \rho g l z^* - \sigma_2)\sqrt{\frac{1+z^*}{1-z^*}} dz^* \\ & + \int_{k_1}^{Z} (p_Q(t) + \rho g l z^* - \sigma_1)\sqrt{\frac{1+z^*}{1-z^*}} dz^* \Bigg\}_{z\to l} \end{aligned} \tag{A.18}$$

and when k_1 approaches unity, the fracture extension pressure for the lower tip corresponds to case 3 in Fig. 3. While when k_3 approaches unity, the fracture extension pressure for the lower tip corresponds to case 2 in Fig. 3.

References

Adachi, J.I., Detournay, E., Peirce, A.P., 2010. Analysis of the classical pseudo-3D model for hydraulic fracture with equilibrium height growth across stress barriers. Int. J. Rock Mech. Min. Sci. 47 (4), 625–639.

Advani, S.H., Lee, T.S., Lee, J.K., 1990. Three-dimensional modeling of hydraulic fractures in layered media: part I—finite element formulations. J. Energy Resour. Technol. 112 (1), 1–9.

Ahmed, U., 1984, January. A practical hydraulic fracturing model simulating necessary fracture geometry, fluid flow and leakoff, and proppant transport. In: SPE Unconventional Gas Recovery Symposium. Society of Petroleum Engineers.

Atkins, A.G., 1979. Cracking of layered structures: the suppression of yielding by cast hardening. Mech. Behav. Mater. 3, 341–349.

Atkins, A.G., Mai, Y.W., 1985. Elastic and Plastic Fracture: Metals, Polymers, Ceramics, Composites, Biological Materials. Halsted Press, Ellis Horwood.

Beremin, F.M., Pineau, A., Mudry, F., Devaux, J.C., D'Escatha, Y., Ledermann, P., 1983. A local criterion for cleavage fracture of a nuclear pressure vessel steel. Metall. Trans. A 14 (11), 2277–2287.

Broek, D., 1991. Elementary Engineering Fracture Mechanics, 4th Revised Edition. Kluwer Academic Publishers, Dordrecht, Netherlands.

Bui, H.D., 1977. An integral equations method for solving the problem of a plane crack of arbitrary shape. J. Mech. Phys. Solids 25 (1), 29–39.

Chen, T., Dvorak, G.J., Benveniste, Y., 1992. Mori-Tanaka estimates of the overall elastic moduli of certain composite materials. J. Appl. Mech. 59 (3), 539–546.

Chuprakov, D., Melchaeva, O., Prioul, R., 2014. Injection-sensitive mechanics of hydraulic fracture interaction with discontinuities. Rock Mech. Rock Eng. 47 (5), 1625–1640.

Clifton, R.J., Abou-Sayed, A.S., 1979, January. On the computation of the three-dimensional geometry of hydraulic fractures. In: Symposium on Low Permeability Gas Reservoirs. Society of Petroleum Engineers.

Clifton, R.J., Abou-Sayed, A.S., 1981, January. A variational approach to the prediction of the three-dimensional geometry of hydraulic fractures. In: SPE/DOE Low Permeability Gas Reservoirs Symposium. Society of Petroleum Engineers.

Dahi-Taleghani, A., Olson, J.E., 2011. Numerical modeling of multistranded-hydraulic-fracture propagation: accounting for the interaction between induced and natural fractures. SPE J. 16 (03), 575–581.

Economides, M.J. (Ed.), 2000. Reservoir Stimulation, vol. 18. Wiley, Chichester.

Eriksson, K., 1998. The effective fracture toughness of structural components obtained with the blend rule. Nucl. Eng. Des. 182 (2), 123–129.

Eriksson, K., Atkins, A.G., 1995. The effective through crack fracture toughness of structural components of older inhomogeneous steels. Mater. Ageing Compon. Life Ext. 1, 147–154.

Eshelby, J.D., 1957, August. The determination of the elastic field of an ellipsoidal inclusion, and related problems. In: Proceedings of the Royal Society of London a: Mathematical, Physical and Engineering Sciences, vol. 241. The Royal Society, pp. 376–396. No. 1226.

Fung, R.L., Vilayakumar, S., Cormack, D.E., 1987. Calculation of vertical fracture containment in layered formations. SPE Form. Eval. 2 (04), 518–522.

Gao, H., Rice, J.R., 1989. A first-order perturbation analysis of crack trapping by arrays of obstacles. J. Appl. Mech. 56 (4), 828–836.

Griffith, A.A., 1921. The phenomena of rupture and flow in solids. Philosophical Trans. R. Soc. Lond. Ser. A, Contain. Pap. a Math. or Phys. character 221, 163–198.

Gu, H., Weng, X., 2010, January. Criterion for fractures crossing frictional interfaces at non-orthogonal angles. In: 44th US Rock Mechanics Symposium and 5th US-Canada Rock Mechanics Symposium. American Rock Mechanics Association.

Gu, H., Weng, X., Lund, J.B., Mack, M.G., Ganguly, U., Suarez-Rivera, R., 2012. Hydraulic fracture crossing natural fracture at nonorthogonal angles: a criterion

and its validation. SPE Prod. Operations 27 (01), 20–26.
Hashin, Z., Shtrikman, S., 1963. A variational approach to the theory of the elastic behaviour of multiphase materials. J. Mech. Phys. Solids 11 (2), 127–140.
Heerens, J., Zerbst, U., Bauschke, H.M., Schwalbe, K.H., 1994. On the Application of the Weakest Link Model in the Lower Shelf and Transition, 2013, February. In ECF10, Berlin.
Hill, R., 1965. A self-consistent mechanics of composite materials. J. Mech. Phys. Solids 13 (4), 213–222.
Hirth, J.P., Lothe, J., 1968. Theory of Dislocations, 780 pp.
Irwin, G.R., 1957. Analysis of stresses and strains near the end of a crack traversing a plate. Spie Milest. Ser. MS 137 (167–170), 16.
Irwin, G.R., 1958. Fracture in "Handbuch der Physik,", vol. V.
Iwadate, T., Tanaka, Y., Ono, S., Watanabe, J., 1983, January. An analysis of elastic-plastic fracture toughness behavior for J IC measurement in the transition region. In: Elastic-plastic Fracture: Second Symposium, Volume II Fracture Resistance Curves and Engineering Applications. ASTM International.
Kachanov, L., 2013. Introduction to Continuum Damage Mechanics, vol. 10. Springer Science & Business Media.
Landes, J.D., Shaffer, D.H., 1980. Statistical characterization of fracture in the transition region. In: Fracture Mechanics. ASTM International.
Li, Y., Zhou, M., 2013. Prediction of fracture toughness of ceramic composites as function of microstructure: I. Numerical simulations. J. Mech. Phys. Solids 61 (2), 472–488.
Meyer, B.R., 1986, January. Design formulae for 2-D and 3-D vertical hydraulic fractures: model comparison and parametric studies. In: SPE Unconventional Gas Technology Symposium. Society of Petroleum Engineers.
Morales, R.H., Brady, B.H., Ingraffea, A.R., 1993, January. Three-dimensional analysis and visualization of the wellbore and the fracturing process in inclined wells. In: Low Permeability Reservoirs Symposium. Society of Petroleum Engineers.
Mori, T., Tanaka, K., 1973. Average stress in matrix and average elastic energy of materials with misfitting inclusions. Acta metall. 21 (5), 571–574.
Newberry, B.M., Nelson, R.F., Ahmed, U., 1985, January. Prediction of vertical hydraulic fracture migration using compressional and shear wave slowness. In: SPE/DOE Low Permeability Gas Reservoirs Symposium. Society of Petroleum Engineers.
Nordgren, R.P., 1972. Propagation of a vertical hydraulic fracture. Soc. Petroleum Eng. J. 12 (04), 306–314.
Olson, J.E., Taleghani, A.D., 2009, January. Modeling simultaneous growth of multiple hydraulic fractures and their interaction with natural fractures. In: SPE Hydraulic Fracturing Technology Conference. Society of Petroleum Engineers.
Palmer, I.D., Carroll Jr., H.B., 1983a. Three-dimensional hydraulic fracture propagation in the presence of stress variations. Soc. Petroleum Eng. J. 23 (06), 870–878.
Palmer, I.D., Carroll Jr., H.B., 1983b, January. Numerical solution for height and elongated hydraulic fractures. In: SPE/DOE Low Permeability Gas Reservoirs Symposium. Society of Petroleum Engineers.
Palmer, I.D., Craig, H.R., 1984, January. Modeling of asymmetric vertical growth in elongated hydraulic fractures and application to first MWX stimulation. In: SPE Unconventional Gas Recovery Symposium. Society of Petroleum Engineers.
Perkins, T.K., Kern, L.R., 1961. Widths of hydraulic fractures. J. Petroleum Technol. 13 (09), 937–949.
Renshaw, C.E., Pollard, D.D., 1995, April. An experimentally verified criterion for propagation across unbounded frictional interfaces in brittle, linear elastic materials. Int J. Rock Mechanics. Min Sci. Geomechanics. Abstr 32 (No. 3), 237–249. Pergamon.
Settari, A., Cleary, M.P., 1986. Development and testing of a pseudo-three-dimensional model of hydraulic fracture geometry. SPE Prod. Eng. 1 (06), 449–466.
Simonson, E.R., Abou-Sayed, A.S., Clifton, R.J., 1978. Containment of massive hydraulic fractures. Soc. Petroleum Eng. J. 18 (01), 27–32.
Slatcher, S., 1986. A probabilistic model for lower-shelf fracture toughness—theory and application. Fatigue & Fract. Eng. Mater. Struct. 9 (4), 275–289.
Sneddon, I.N., Elliott, H.A., 1946. The opening of a Griffith crack under internal pressure. Q. Appl. Math. 4 (3), 262–267.
Valko, P.P., Liu, S., 2015. February. An improved equilibrium-height model for predicting hydraulic fracture height migration in multi-layered formations. In: SPE Hydraulic Fracturing Technology Conference. Society of Petroleum Engineers.
Wallin, K., Saario, T., Törrönen, K., 1984. Statistical model for carbide induced brittle fracture in steel. Metal Sci. 18 (1), 13–16.
Walpole, L.J., 1981. Elastic behavior of composite materials: theoretical foundations. Adv. Appl. Mech. 21, 169–242.
Warpinski, N.R., Teufel, L.W., 1987. Influence of geologic discontinuities on hydraulic fracture propagation (includes associated papers 17011 and 17074). J. Petroleum Technol. 39 (02), 209–220.
Weng, G.J., 1984. Some elastic properties of reinforced solids, with special reference to isotropic ones containing spherical inclusions. Int. J. Eng. Sci. 22 (7), 845–856.
Willis, J.R., 1981. Variational and related methods for the overall properties of composites. Adv. Appl. Mech. 21, 1–78.
Wu, K., 2014. Mechanics Analysis of Interaction between Hydraulic and Natural Fractures in Shale Reservoirs. Unconventional Resources Technology Conference (URTEC).
Zhou, J., Chen, M., Jin, Y., Zhang, G.Q., 2008. Analysis of fracture propagation behavior and fracture geometry using a tri-axial fracturing system in naturally fractured reservoirs. Int. J. Rock Mech. Min. Sci. 45 (7), 1143–1152 (SS).
Zhou, J., Huang, H., Deo, M., 2015, November. Modeling the interaction between hydraulic and natural fractures using dual-lattice discrete element method. In: 49th US Rock Mechanics/Geomechanics Symposium. American Rock Mechanics Association.